Hindawi
Modelling and Simulation in Engineering
Volume 2018, Article ID 4239725, 19 pages
https://doi.org/10.1155/2018/4239725

Research Article

From Antenna Design to High Fidelity, Full Physics Automotive Radar Sensor Corner Case Simulation

Ushemadzoro Chipengo,[1] **Peter M. Krenz**,[2] **and Shawn Carpenter**[3]

[1]*ANSYS Inc., Ann Arbor, MI 48108, USA*
[2]*ANSYS Inc., Evanston, IL 60201, USA*
[3]*ANSYS Inc., Urbana-Champaign, IL 61801, USA*

Correspondence should be addressed to Ushemadzoro Chipengo; ushe.chipengo@ansys.com

Received 29 August 2018; Accepted 8 November 2018; Published 27 December 2018

Academic Editor: Aiguo Song

Advanced driver assistance systems (ADAS) have recently been thrust into the spotlight in the automotive industry as carmakers and technology companies pursue effective active safety systems and fully autonomous vehicles. Various sensors such as lidar (light detection and ranging), radar (radio detection and ranging), ultrasonic, and optical cameras are employed to provide situational awareness to vehicles in a highly dynamic environment. Radar has emerged as a primary sensor technology for both active/passive safety and comfort-advanced driver-assistance systems. Physically building and testing radar systems to demonstrate reliability is an expensive and time-consuming process. Simulation emerges as the most practical solution to designing and testing radar systems. This paper provides a complete, full physics simulation workflow for automotive radar using finite element method and asymptotic ray tracing electromagnetic solvers. The design and optimization of both transmitter and receiver antennas is presented. Antenna interaction with vehicle bumper and fascia is also investigated. A full physics-based radar scene corner case is modelled to obtain high-fidelity range-Doppler maps. Finally, this paper investigates the effects of inclined roads on late pedestrian detection and the effects of construction metal plate radar returns on false target identification. Possible solutions are suggested and validated. Results from this study show how pedestrian radar returns can be increased by over 16 dB for early detection along with a 27 dB reduction in road construction plate radar returns to suppress false target identification. Both solutions to the above corner cases can potentially save pedestrian lives and prevent future accidents.

1. Introduction

The vehicle of the future is slated to be a mobile and intelligent technology hub equipped with full autonomous driving capabilities and active safety systems that will provide comfort and convenience while making tomorrow's roads safer. While fully autonomous vehicles have emerged as a driving force behind the recent automotive industry ADAS revolution, an even more immediate goal is to make today's roads safer. Surveys show that 90% of accidents are due to human errors [1]. Partners of Advanced Transit Highways (PATH) estimated that car accidents and their associated damages are almost 3% of the world's gross domestic products in cost [1]. In 2016, 40 000 people in the United States alone and more than 1.25 million people worldwide lost their lives in car accidents [2]. In March 2010, the United Nations General Assembly declared the years 2011 to 2020 as the "*Decade of Action for Road Safety*." Carmakers have responded by equipping vehicles with active safety systems which fall under the wider umbrella of ADAS. Compared with passive safety systems such as airbags that only deploy after a crash, active safety systems are constantly monitoring the vehicle's environment and can automatically control the vehicle to avoid a collision [3]. Various sensor technologies are used to map the immediate environment of the vehicle while also providing it with its position and velocity in relation to other vehicles on the road. Optical cameras [4–7], lidar, radar, and ultrasonic sensors are the most widely used sensors. Optical cameras can provide high-definition images; however, they are expensive, require significant computer processing, and cannot provide range information. Lidar systems can provide high-resolution, 3D

images. On the other hand, lidar systems are expensive and are adversely affected by vehicle vibration and by weather conditions such as rain and snow. Lidar systems are also limited to observation of "first bounce" objects and cannot detect obscured objects. Ultrasonic sensors are low cost, can operate in the dark, and are not affected by the color of targets; however, they have very limited range, typically below 10 meters. While the car of the future will most likely have all these sensors, radar has emerged as a clear front runner in automotive active safety sensors. This is because radar is inexpensive, robust, can detect the presence of obscured objects, and can simultaneously provide the range and velocity of multiple targets without being adversely affected by weather and lighting conditions [8].

Automotive radars are broadly grouped as corner and front radars. The corner radar systems are responsible for blind spot detection (BSD), rear cross traffic alert (RCTA), and lane change assist (LCA). Front radars are usually mid- to long-range radars that are used for adaptive cruise control (ACC) and automatic emergency braking (AEB). Some radar systems are placed on the sides of vehicles for precrash alerts [9–11]. Figure 1 shows some of the common automotive radar applications. This paper will focus on the long-range adaptive cruise control radar system. Ultrasonic sensors are typically used for vehicle parking assistance. However, ultrawide band (UWB), short-range radars with high-range resolution and accuracy are needed for fully autonomous vehicle parking.

Current automotive radar systems are designed at 24 GHz and 77 GHz. The 24 GHz frequency band (24 GHz to 24.25 GHz) has a narrow band (250 MHz) for industrial, scientific, and medical applications. An ultrawide band (UWB) for radar applications exists from 21.65 GHz to 26.65 GHz (5 GHz bandwidth). Recent regulation moves by the Federal Communications Commission (FCC) and the European Telecommunications Standards Institute (ETSI) will see the removal of the UWB (21.65–26.65 GHz), leaving only the narrow band (250 MHz). Starting from January 1, 2022, the 24 GHz UWB will no longer be available. On the other hand, the 77 GHz band has a 76- to 77 GHz band for long-range adaptive cruise control (ACC) and 77–81 GHz for high-resolution, short-range radar. Therefore, when compared with 24 GHz, 77 GHz is an attractive option for all future automotive radar systems due to its superior range accuracy, range resolution, velocity accuracy, and velocity resolution. Specifically, due to the higher frequency of operation and larger bandwidth, 77 GHz radar can have up to 20 times better range resolution and 3 times the velocity accuracy of remaining narrowband 24 GHz systems. Another consideration is the practical bandwidths of the components (amplifiers, LNAs, etc.), which typically have an operational fractional bandwidth (5%–10%) which is greater in actual bandwidth at 77 GHz (by a factor of 3) over that of 24 GHz. Antenna size scales inversely with frequency; therefore, the antenna size can be reduced by approximately 3 times when operating at 77 GHz compared with 24 GHz [12].

As radar systems evolve from merely being able to warn a driver as they operate the vehicle to actively controlling the vehicle (adaptive cruise control), these systems will need to be extensively tested and validated for reliability. It is estimated that billions of miles will need to be driven in testing to demonstrate the reliability of autonomous vehicles. Furthermore, engineers will need to test these radar sensors in corner cases. Specifically, there are outlying cases where interesting phenomena such as ghost targets, radar blinding, and disappearing targets can occur. Companies and researchers routinely build and test radar systems [3, 8, 10, 11, 13, 14]. Testing radar systems in corner cases can also be impossible in some cases since automotive companies would never knowingly drive a validation AV through a scenario where they could get the driver or other people killed in real life.

Recently, emphasis has been placed on the salient issues that plague automotive radar systems in a bid to make the systems robust for fully autonomous operation [15–20]. Specifically, researchers have investigated the effects of rain clutter, antenna beam expansion, guardrail detection, algorithms for direction of arrival, and noise filtering for radar systems in tunnels. Although a lot of research has already been done, none of these studies have used full physics simulation to investigate the multitude of possible variations of operating conditions that could affect the normal operation of the radar system.

Due to a multitude of radar corner cases and operating situations, it is both expensive and time consuming to build and test radar systems. Simulation is the only practical approach as it allows the radar sensor designer to develop and test radar sensors in a short space of time. Entire products can be designed, tested, and optimized in simulation before a single fabrication cycle begins, thus reducing development cost, improving reliability, and significantly reducing the time to market. Antenna design, antenna performance on car platform, radar system, and corner case testing are the key areas of interest in radar system development. Radar scene and corner case testing are typically done via fabrication and field testing. A reason for this is the extremely large electrical size of radar scenes (usually hundreds of billions of cubic wavelengths in size at 77 GHz) that make it impractical for simulation with finite element method- (FEM-) based electromagnetic solvers.

In this paper, an entire, full physics-based, 77 GHz automotive radar simulation workflow will be presented. Specifically, in Section 2, the design and optimization of transmitting and receiving antennas will be accomplished using ANSYS's finite element method (FEM)-based High Frequency Structure Simulator (HFSS-FEM). In Section 3, the performance of these antennas when mounted on a car bumper and fascia will be investigated using ANSYS's shooting and bouncing (SBR+) ray solver (HFSS-SBR+). A full radar scene will be modelled and solved using HFSS SBR+ in Section 4. Finally, some corner cases will be investigated in Section 5. Specifically, terrain-induced reduction of radar returns will be investigated and mitigated. Proposed mitigation methods predict a 16-dB (~40x) enhancement in target visibility. Such enhancements will be shown to improve pedestrian detection on inclined roads. Finally, the emergence of ghost targets that emanate from diffraction-induced strong radar returns of metallic construction plates will be investigated. These ghost targets are

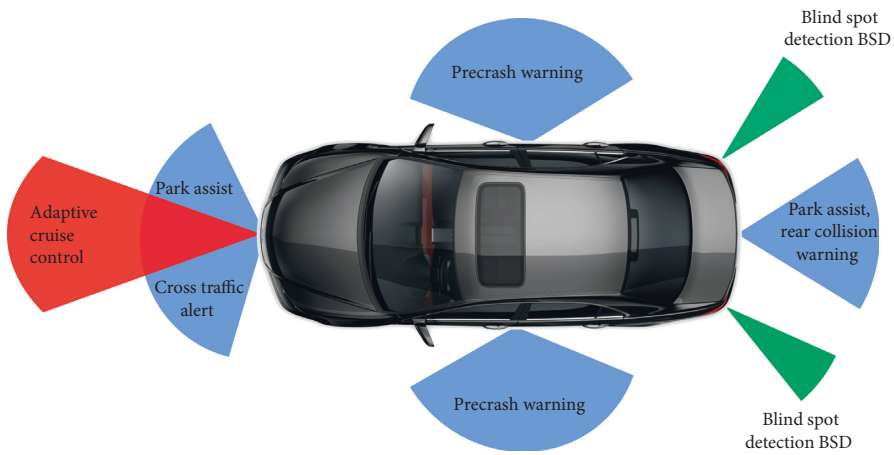

Figure 1: Advance driver assistance system (ADAS) radars. Automotive radar systems will predominantly function at 77 GHz as 24 GHz is phased out. This paper focuses on the long-range adaptive cruise control radar system.

problematic as they can confuse the radar system and engage the automatic emergency braking (AEB) system of a vehicle. A method for reducing the returns of construction plates by more than 27 dB (500x) is also presented. Such simulation-based solutions have the potential to save lives and prevent future accidents. To the best of our knowledge, this is the first full physics-based antenna-to-scene simulation work that has been presented.

2. Antenna Design and Optimization

2.1. Choosing Appropriate Numerical Methods and Theories for Analysis. In this paper, two main numerical techniques will be used to conduct a full electromagnetic analysis of the 77 GHz automotive radar. Specifically, the finite element method (FEM) and the shooting and bouncing rays (SBR+) techniques will be employed. FEM determines the electromagnetic field solution by discretizing the entire geometry under analysis into finite-sized tetrahedral elements. Using the differential form of Maxwell's equation, the fields in each tetrahedral are represented by local basis functions. SBR+ is a hybrid electromagnetic solver that uses geometrical optics (GO) to trace the paths of transmitted electromagnetic rays. Whenever these rays are incident on geometries, SBR+ uses physical optics (PO) to "paint" currents on these geometries. These currents are then reradiated into free space. SBR+ accounts for reflection, refraction, and diffraction of electromagnetic waves. For more details on Maxwell's equations, physical optics (PO), geometrical optics (GO), diffraction, reflection, and refraction, the interested reader is referred to [21].

The FEM technique is ideal for electrically small problems typically 1–10λ in size (λ is the wavelength of the electromagnetic wave in the solution space), with complex geometrical variations. This is because FEM discretizes and explicitly solves Maxwell's equation for the entire solution space. FEM, however, does not scale efficiently with larger problems that are tens to hundreds of wavelengths in size. SBR+ is an asymptotical solver that is ideal for electrically large problems due to its ray tracing and physical optics techniques. SBR+ can solve problems that are tens to tens of thousands of wavelengths in size. Therefore, in this paper, we will leverage the FEM technique to design the electrically small and geometrically complex antenna sensors. SBR+ will then be used to solve for the electromagnetic response of electrically large, full-scale radar scenes (typically billions of cubic wavelengths in size). SBR+ will also be used to determine the installed radiation patterns of the antennas when mounted on the bumper and fascia, which are extremely large at 77 GHz (1 wavelength at 77 GHz is approximately 4 mm).

2.2. Design and Optimization of Series-Fed Microstrip Patch Antenna Arrays. Radar determines the range and velocity of targets in a given scene by sending modulated electromagnetic pulses and observing the time-delayed reflected signals. Antennas are thus integral components in radar systems as they are responsible for sending and receiving electromagnetic waves. Various antenna designs have been proposed for 77 GHz radar systems. Specifically, slotted waveguide, reflector, lens, and microstrip patch antennas have been developed for automotive radar [22, 23]. However, the microstrip patch antenna has emerged as the leading topology choice due to its simple structure, low profile, ease of integration with systems, and low manufacturing cost [24]. A popular variant of the microstrip patch antenna is the microstrip series-fed patch antenna array [25–28].

The series-fed linear array is analyzed using the modified transmission line model. Figure 2 shows a single super element that consists of multiple rectangular microstrip patch antennas [25, 29]. This single super element will be used as the transmitting antenna. The model shown in Figure 2 is a modified version of Derneryd's transmission line model. In this model, the microstrip patch antenna is being represented by two slots that are responsible for radiation (boxed in red). These radiating slots on both sides of the patch are represented by parallel conductance G and susceptance B. Although this model works well for a single patch antenna, it falls short when multiple patches are placed in series and fed by a high-impedance feed line. This is because the patch antenna themselves can be viewed as low-impedance

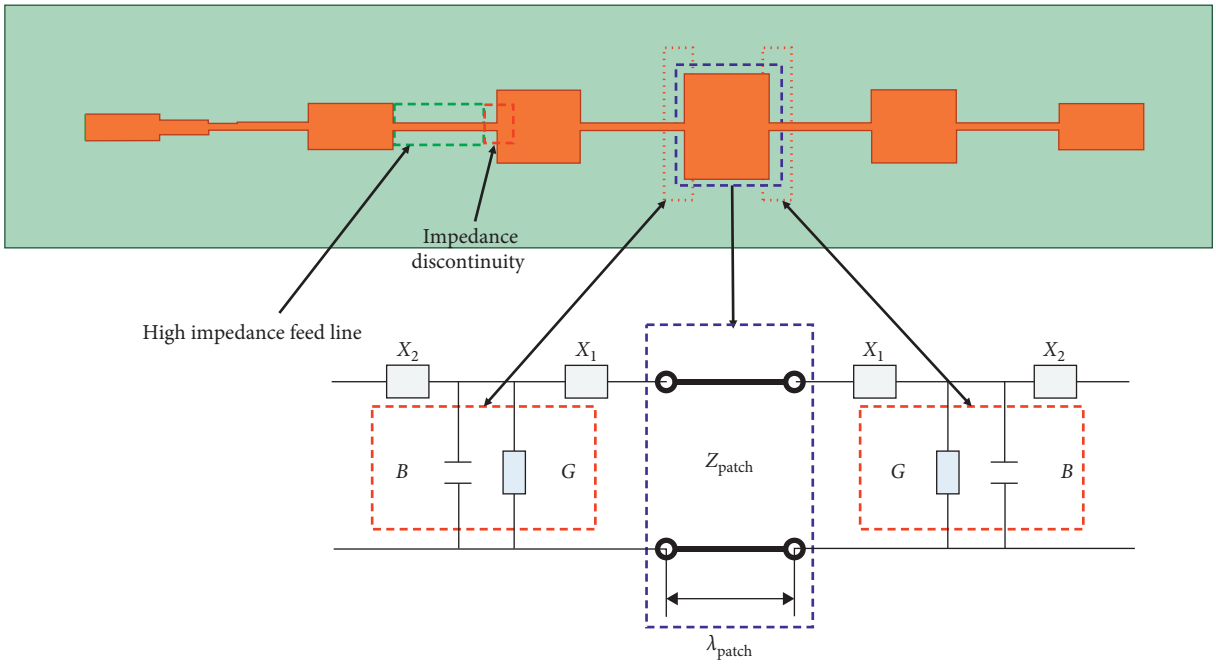

Figure 2: Series-fed microstrip patch array antenna and the modified transmission line model [29]. The radiating slots on both sides of the patch are represented by parallel conductance G and susceptance B. The impedance discontinuity is represented by two additional reactances X_1 and X_2.

transmission line sections. Therefore, the region where the feed line and patch antenna meet represents an impedance discontinuity as shown in Figure 2. This impedance discontinuity is represented by two additional reactances X_1 and X_2.

Although analytical models can provide quick approximate solutions for canonical problems, they typically cannot provide accurate solutions for complex problems. In some cases, an analytical model may not even exist. To analyze the radiation characteristics of complex antenna structures, a full-wave electromagnetic solver that solves either the integral or differential form of Maxwell's equations is required.

HFSS is a finite element method (FEM)-based electromagnetic solver. Using equations and techniques detailed in [25, 29, 30], the antenna was designed and modelled in ANSYS HFSS using a 127-μm thick dielectric layer (RT-Duroid 5880 ε_r = 2.2) and a-9 μm copper cladding. The antenna properties of interest in this design process were the side-lobe level, peak realized gain, and return loss at 77 GHz. Specifically, low side lobes are desired (typically −15 dB) to discriminate true target returns from ground-induced clutter returns. The final antenna design was obtained using parametric and derivative-based optimization in HFSS FEM. The realized gain and far-field radiation pattern of the antenna in Figure 2 are shown in Figure 3.

As previously mentioned, the antenna design in Figure 2 is a transmitting antenna. An array of 4 transmitting antenna super elements was constructed to create the receiving (RX) antenna. Further side lobe suppression was achieved by excitation amplitude tapering for each of the super elements with normalized voltage excitations of 1 V, 1.73 V, 1.73 V, and 1 V. Figure 4 shows the realized gain and the far-field radiation pattern of the receiving (RX) antenna. Figure 5 shows the return loss of the transmitting antenna and the receiving antenna when all the elements are excited.

3. Antenna Packaging and Placement Effects

Electromagnetic wave propagation is affected by the presence of conductors and dielectrics. Specifically, metallic or dielectric materials near the antenna can significantly modify the antenna characteristics. Unfortunately, these modifications typically have adverse effects such as gain reduction, side-lobe level increase, beam misalignment, and impedance mismatch. Antenna engineers are not only concerned about the antenna design but also about the antenna placement and packaging as these have a significant impact the antenna performance. At 77 GHz, phase errors stemming from antenna packaging and placement effects can lead to errors in target identification and characterization.

In a highly competitive market, carmakers are constantly trying to improve the visual appeal of vehicles while adding more functional technology. In addition, other factors such as aerodynamics must be considered when designing the facia and body of high end vehicles. Sometimes functionality can clash with the aerodynamic and aesthetic needs of the carmaker. An example of this is the current generation of lidar systems and cameras that are mounted on top of trial autonomous vehicles. Although these sensors have an indispensable role to play in autonomous vehicle operation, they require optical line-of-sight and are neither aesthetically pleasing nor aerodynamic. Radar, however, can be integrated more seamlessly into vehicles by mounting the radar sensors behind the vehicle facia. However, this is not a process without its own challenges as the properties of the metallic bumper and dielectric facia can significantly alter the antenna properties.

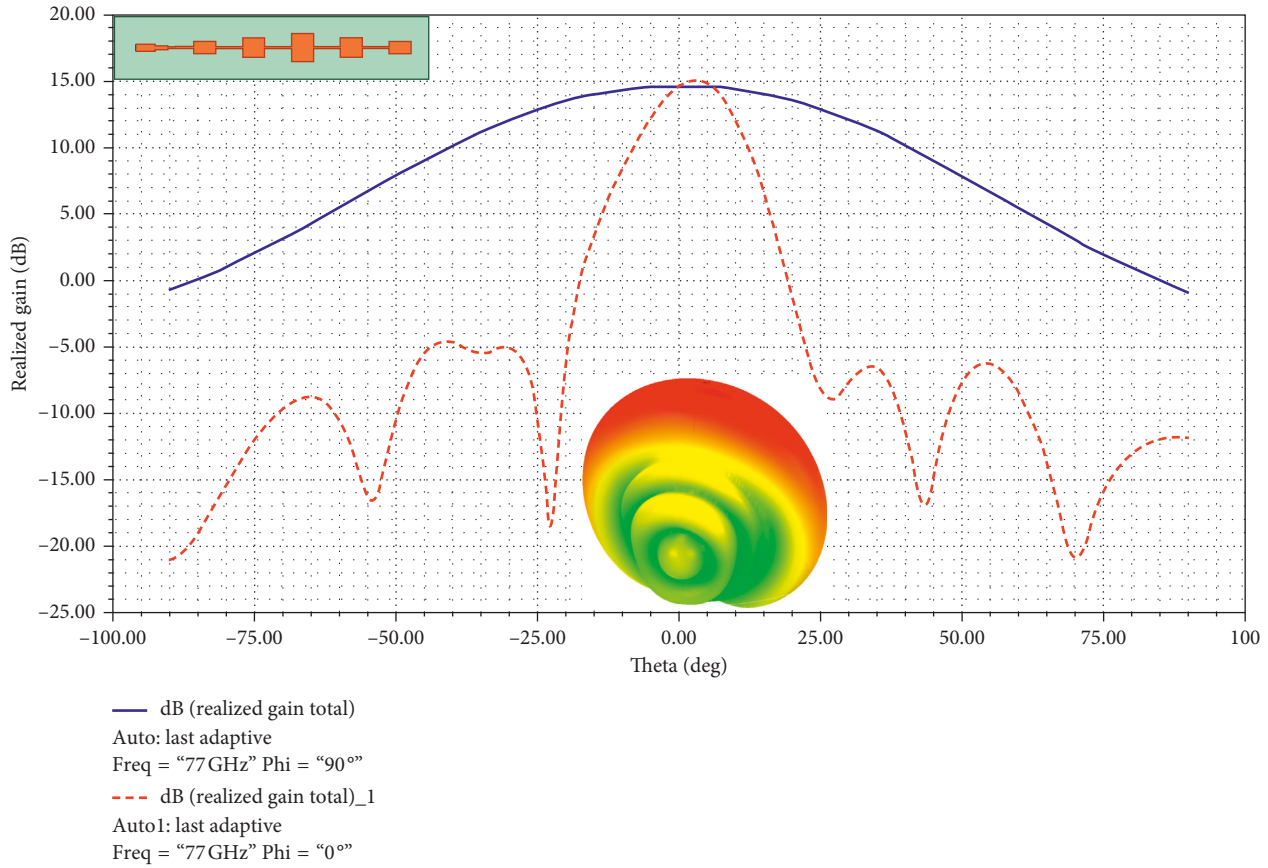

Figure 3: Realized gain (dB) of the transmitting (TX) antenna with an insert of the antenna design and full far-field radiation pattern.

To meet design specifications, engineers need to account for antenna packaging, bumper, and facia effects on the overall radar sensor performance. If the radar sensor cannot meet the required specifications, automotive radar companies estimate the cost of repeating the packaging at around $1 million per cycle [31]. Furthermore, package redesign can lead to delays in the vehicle launch itself, leading to huge losses for the carmakers. Additionally, unaccounted platform and packaging effects during vehicle operation can cause accidents, loss of life, and disastrous liability issues for carmakers.

In the past, the effects of antenna placement and packaging were investigated by fabricating the antenna, packaging it, and placing it behind the facia for measurement. This was a process that required back and forth interaction between the radar sensor manufacturer and the vehicle manufacturer. Indeed, such a process was trial and error and extremely iterative, taking up to nine months in product development. Specifically, a late change in the paint type or facia design of the vehicle would have to be accounted for by building the new vehicle and placing the antenna behind the new platform [32]. Today, simulation has emerged as the most efficient way to investigate the effects of antenna placement and packaging. In simulation, the engineer simply acquires bumper and facia computer-aided designs (CAD) from the vehicle original equipment manufacturer (OEM). Using these CAD files, the antenna can be simulated in the exact place where it would be located in normal vehicle operation.

Effects of a dielectric cover, bumper, and facia on the radiation characteristics of the antenna from Section 2 were investigated using HFSS FEM and HFSS SBR+. Specifically, the effects of the dielectric package were accounted for by solving for the entire antenna and dielectric package using HFSS-FEM. Simulating bumper and facia effects can be challenging with an FEM solver due to the electrical size of the problem. At 77 GHz, electromagnetic waves have a wavelength of around 4 mm, thus making a typical vehicle facia and bumper very electrically large when compared with this wavelength. Solving for such a large problem can become computationally expensive and time consuming using finite element method solvers (FEM). Figure 6 shows the simulation workflow from the isolated antenna to the packaged and mounted antenna.

HFSS SBR+ is a high-frequency asymptotic ray-tracing electromagnetic solver. SBR+ is a physical optics (PO) solver that uses geometrical optics (GO) ray tracing to efficiently solve for electrically large geometries. In SBR+, rays from the antenna source are "shot" into space in all directions, some of these rays exit the computational domain unhindered, whereas some bounce off or through the geometry. Using PO and GO approximations, equivalent surface currents are then "painted" on the geometry. These equivalent surface currents are then radiated to observation points or angles where a summation of all incident and scattered fields is calculated. The process is performed for each of the rays until they either exit the domain or reach their user-defined maximum number of bounces [33].

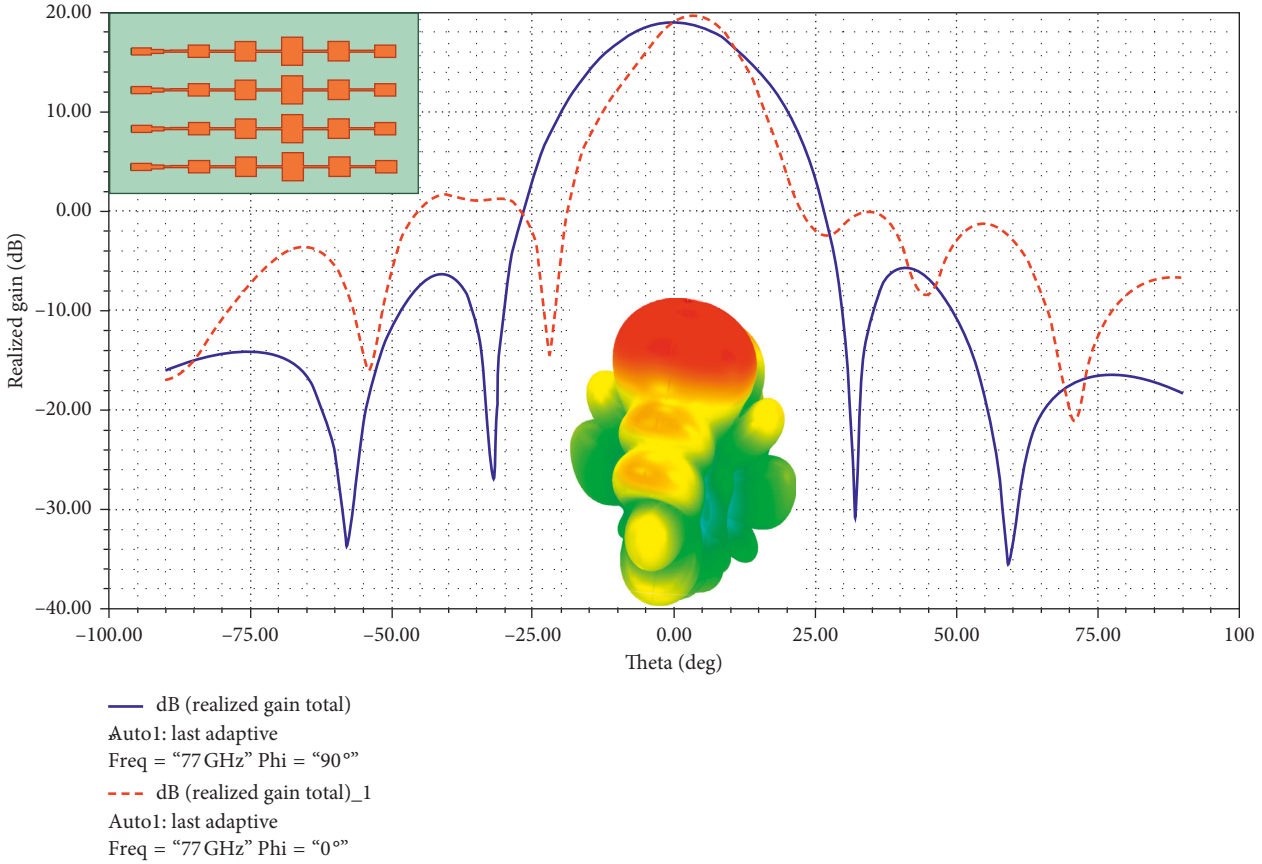

Figure 4: Realized gain (dB) of the receiving (RX) antenna with an insert of the antenna design and full far-field radiation pattern.

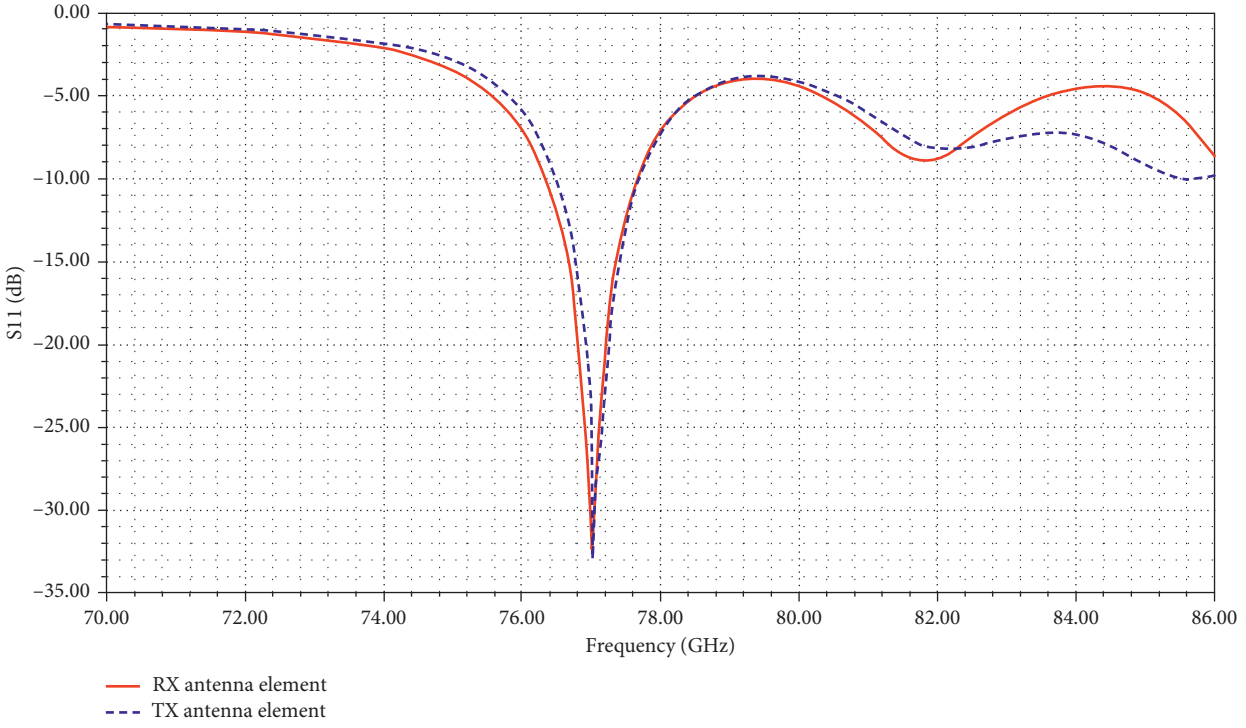

Figure 5: Return loss of the transmitting antenna and one of the elements of the receiving antenna when all the elements are excited.

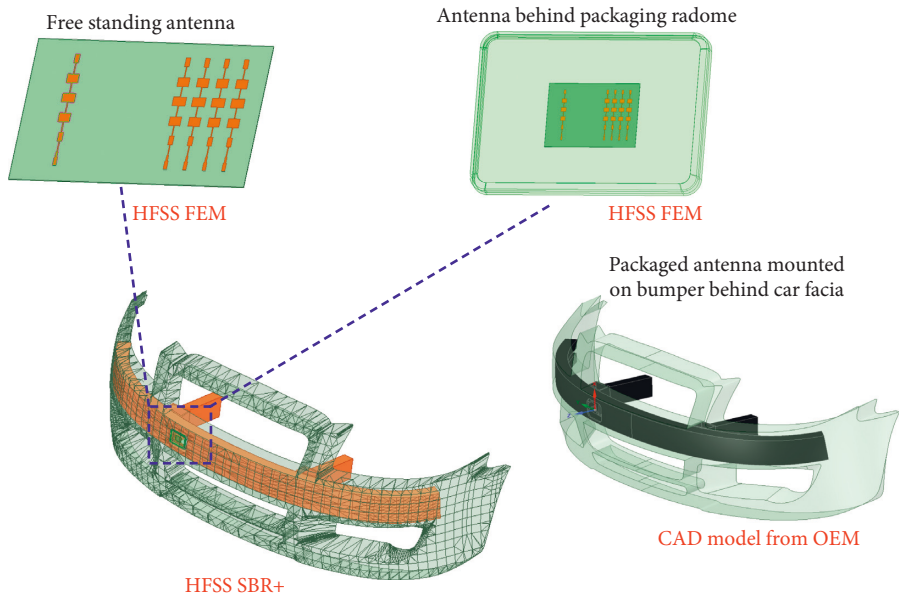

Figure 6: Antenna packaging and mounting on car bumper and facia. Stand-alone and packaged antennas can be simulated in HFSS FEM. The full antenna on bumper/facia simulation uses SBR+.

Using HFSS SBR+, CAD models of the packaged antenna, bumper, and facia were imported and setup as shown in Figure 6. The effects of antenna packaging and integration on vehicles are shown in Figures 7 and 8 for the transmitter and receiver antennas, respectively. This investigation shows that antenna packaging and integration on the vehicle platform can lead to more than 4 dB loss in the realized gain along with a modification of the far-field radiation pattern. The antenna side-lobe level is also increased by more than 6 dB, leading to possible amplification of ground clutter returns.

4. Full Physics Radar Scene Modelling and Simulation

The operating principle behind radar is that objects reflect incident electromagnetic waves. Radar sensors determine the distance (range) and velocity of objects by emitting electromagnetic signals and waiting for reflected signals. Radar topics have been extensively covered in literature; the interested reader is referred to [14, 34, 35]. All radar systems typically seek to determine some or all the attributes of a target, namely, range, velocity, and direction of arrival (DOA). It is the nature of the emitted electromagnetic signal and the subsequent digital signal processing that differentiates radar systems. Pulsed continuous wave, frequency-modulated continuous wave (FMCW), stepped frequency continuous wave (SFCW), and orthogonal frequency division multiplexing (OFDM) are some variants of radar implementation [9]. A popular implementation of radar in automotive radar is FMCW or linear frequency modulation. In FMCW, the signal is a chirp signal and it is used for range and velocity determination. The chirp is a signal whose frequency linearly increases with time in a transmission cycle. Range is determined by observing the frequency difference between the transmitted signal and the time-delayed reflected signal. In the positive frequency ramp segment of the signal, the reflected signal is lower in frequency due to the time delay. The difference frequency is found by mixing the received signal with the transmitted signal. A Fourier transform of this intermediate frequency signal reveals different frequency peaks corresponding to different targets at different ranges. To separate the targets in velocity as well, multiple chirps are needed to carry out a second fast Fourier transform (FFT) called a Doppler-FFT [35].

System-level simulations of radar can provide some insight on the feasibility of a radar design and the plausibility of the proposed digital signal processing methods. However, these system-level simulations are not full physics based. This means that system-level simulations do not actually simulate the propagation of electromagnetic waves along with the complex scattering phenomenon such as diffraction. With such a limitation, system-level simulators cannot be used to investigate crucial corner cases. As previously mentioned, efficient full physics simulation of electromagnetic problems is extremely dependent on the electrical size of a problem. A typical radar scene at 77 GHz can be hundreds of billions of cubic wavelengths in size, thus making it impossible for FEM solvers. HFSS SBR+ is a high-frequency, asymptotic electromagnetic solver that uses a physical optics (PO) solution enhanced by geometrical optics (GO) ray tracing to efficiently analyze these electrically large problems.

4.1. Validation of SBR+. HFSS SBR+ can be used to solve radar scene problems using a slight variant of the FMCW technique called the frequency-modulated interrupted continuous-wave radar (FMiCW) [36]. Each radar problem can essentially be described as an antenna coupling problem in the presence of a scattering radar target. To validate the SBR+ approach, TX and RX far-field antenna patterns from the packaged and mounted antenna were imported into an

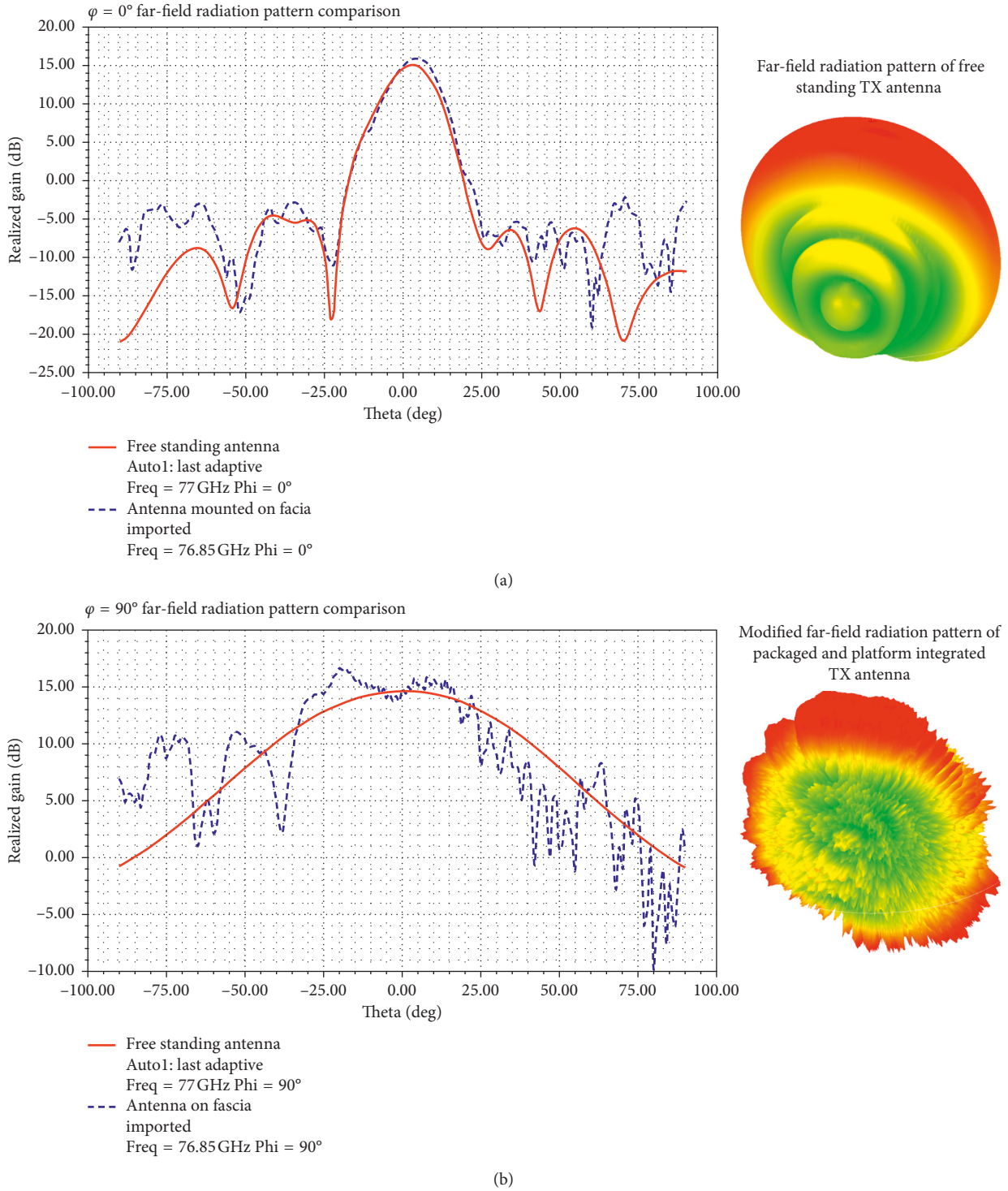

Figure 7: Modification of transmitting (TX) antenna radiation characteristics by packaging and platform integration. The bumper and facia significantly change the far-field radiation pattern.

HFSS SBR+ solution setup in ANSYS Electronics Desktop 19.2 (AEDT). A 2-meter radius metallic sphere was placed in the scene to compare analytical and simulated SBR+ results. The radar equation (1) can be used to predict the received power from a scattering target when its radar cross section (RCS) is known. Conversely, it can be used to determine the RCS of a target when the received power is known.

$$P_r = \frac{P_t G_t G_r \lambda^2 \sigma_{RCS}}{(4\pi)^3 r^4}. \quad (1)$$

Here, $P_r, P_t, G_t, G_r, \lambda, \sigma_{RCS}$, and r refer to the received power, transmitted power, transmitting antenna gain, receiving antenna gain, wavelength, target radar cross section, and range (distance from the target). The setup is shown in Figure 9.

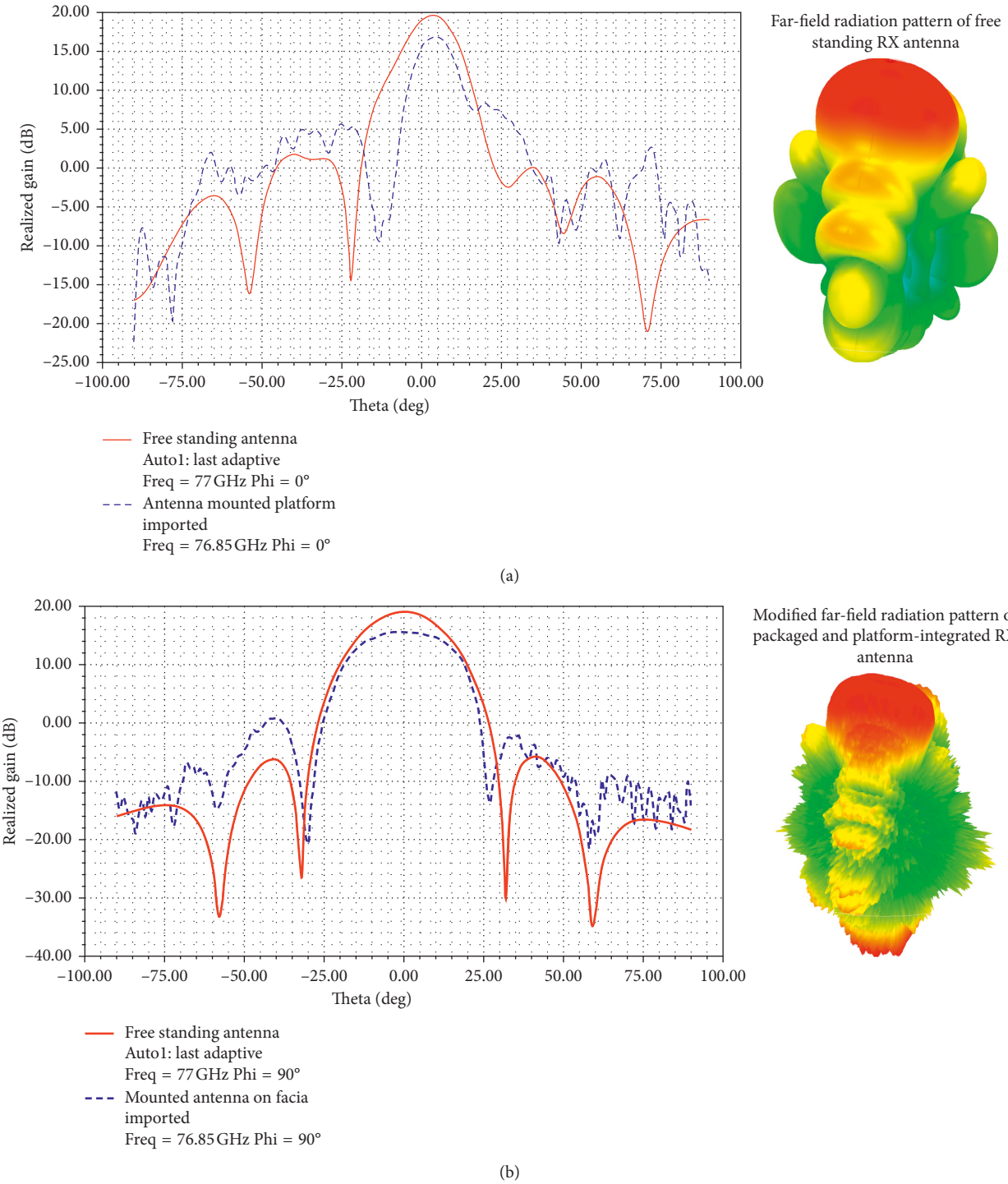

Figure 8: Modification of receiving (RX) antenna radiation characteristics by packaging and platform integration. The bumper and facia significantly change the far-field radiation pattern.

From the simulation shown in Figure 9, HFSS SBR+ predicts that the scattered power received by the RX antenna is −109.42 dBW, whereas the theoretical value is −108.13 dBW. The simulated range of the sphere is 48.375 m. This range is also very accurate since received radar returns are also coming from the leading face of the sphere which is 48 meters away from the radar due to a 2-meter sphere radius.

4.2. Radar Scene Modelling. Each automotive radar simulation has three fundamental components: these are the ego vehicle, actors, and the scene. The scene refers to all the stationary objects such as the road, trees, and streetlights, whereas the actors are all the moving objects such as pedestrians and vehicles. The ego vehicle is the vehicle with the mounted radar. Using HFSS SBR+, a full-scale radar scene

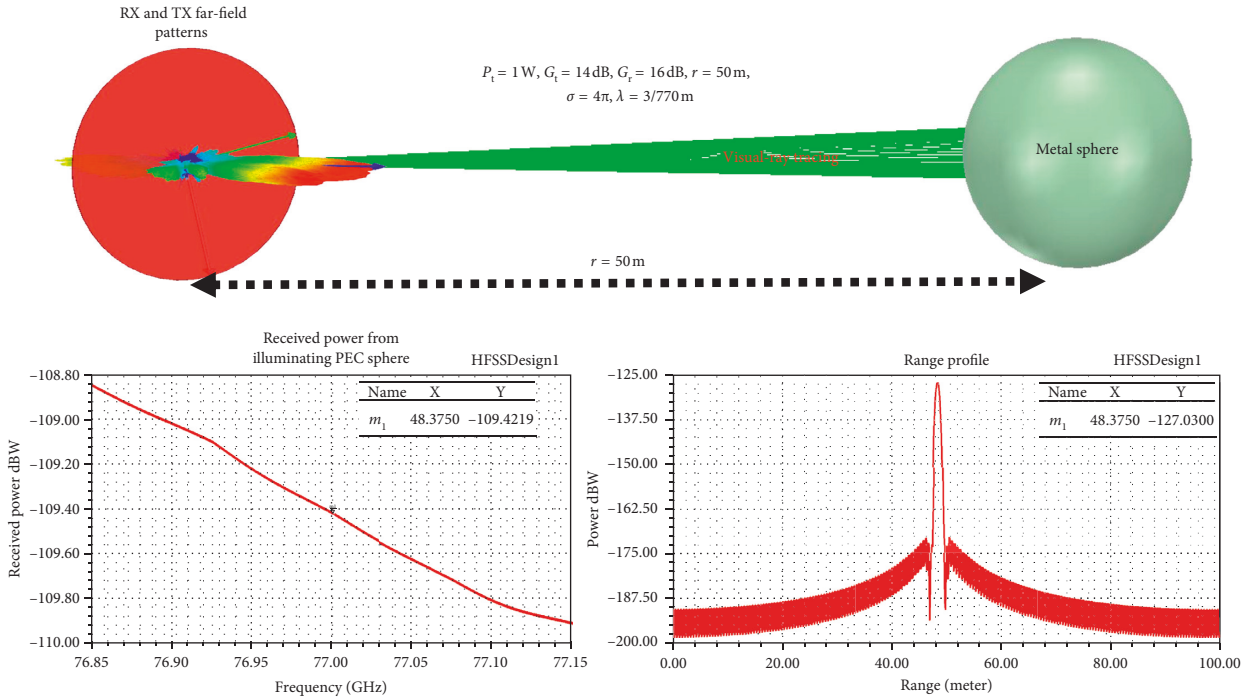

Figure 9: SBR+ validation setup in HFSS SBR+. Imported RX and TX antennas are used to interrogate and receive scattered returns from a metal sphere at 2 GHz. Received power and simulated range are shown in the figures below.

was modelled. The scene included an asphalt road, pedestrians, vehicles, street signs, and street lights.

The vehicles were predominantly modelled as perfect electrical conductors (PEC). Pedestrians were modelled using a single material dry skin human model [37, 38] where the relative dielectric constant and conductivity are $\varepsilon_r = 6.6$ and $\sigma = 38.38$ S/m, respectively. Table 1 shows the radar properties. Figure 10 shows a fully parametrized, to scale model of a radar scene that will be analyzed in HFSS SBR+. The ego vehicle is represented by the transmit and receive antenna patterns that were obtained in the previous chapter, which include the fascia, bumper, and packaging interaction effects. These antenna patterns were imported into this scene for the radar analysis.

HFSS SBR+ solves radar problems using frequency-modulated interrupted continuous wave (FMiCW). In each pulse, the transmitter will ramp up the frequency from 76.85 GHz to 77.15 GHz. After this pulse is emitted, the transmitter will be shut off for a short time, whereas the receiver antenna receives the scattered signal. It is important to note that the receiver is continuously sampling frequencies, whereas the transmitter is ramping the chirp. To obtain a range-Doppler map, the coupled S-parameters of a single frequency sweep (pulse) are loaded into a 1 D array. An inverse fast Fourier-transform (IFFT) is then carried out to give time domain data that can be easily converted into a range profile since the propagation speed of electromagnetic waves in free space is known ($c = 3 \times 10^8$ m/s). The range profiles are then each loaded as rows of the radar data matrix. Once all the required pulses have been loaded into the radar data matrix, a fast Fourier-transform (FFT) is then done along each column to obtain the range-Doppler map.

The range-Doppler map isolates targets in a 2-dimensional space of velocity and distance. In the figures that follow, each

Table 1: Radar parameters for simulation setup.

Parameter	Value
Center frequency	77 GHz
Start frequency	76.85 GHz
Stop frequency	77.15 GHz
Bandwidth	300 MHz
Range resolution	0.5 m
Velocity resolution	1 m/s
Maximum range	100 m
PRF	41.07 kHz
No. of pulses	80
Velocity period	80 m/s

of the range-Doppler maps will show the velocity in the y-axis and range in the x-axis. The color scale relates to the intensity of the reflected signal in dBW. Specifically, the red regions represent stronger radar returns, whereas the blue regions represent areas in space where no target is present or with extremely weak radar returns. Using this color scale, it can be seen that intensity of the reflected signal in dBW depends on the proximity of the target to the ego vehicle and the target's radar cross section (RCS). Another plot of interest that will be shown in the coming section is the radar range plot. The radar range plot isolates targets in a 1-dimensional space. Specifically, the radar range plot only shows the distance of the target from the ego vehicle. The intensity of the reflected signal in dBW is shown in the y-axis, whereas its corresponding distance in meters is shown in the x-axis. Figure 11 shows a range-Doppler map that has been overlaid with its corresponding actors for easy identification.

Figure 11 is a range-Doppler map obtained from a full physics simulation. A lot of insight into how the actual radar sensor "views the world" can be obtained from these types of

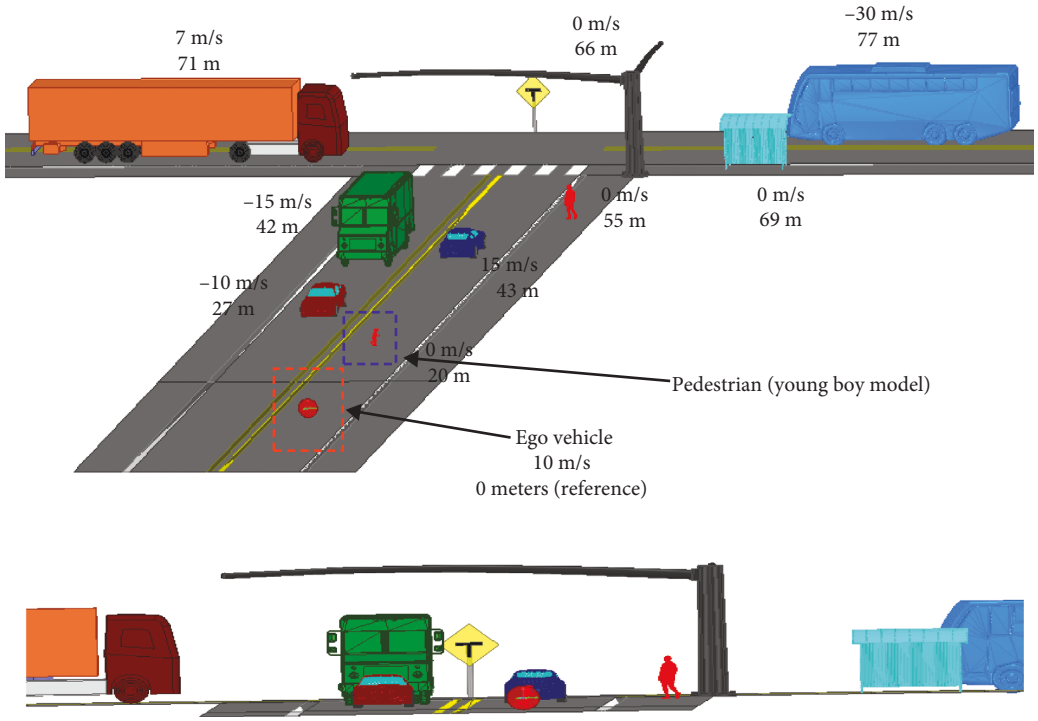

Figure 10: Fully parametrized, to scale model of a radar scene. In this scene, the target velocity and range are written next to it. Of interest is the small boy playing in the middle of the road, 20 meters away from the ego vehicle. The radar sensor (TX/RX) is mounted on the ego vehicle.

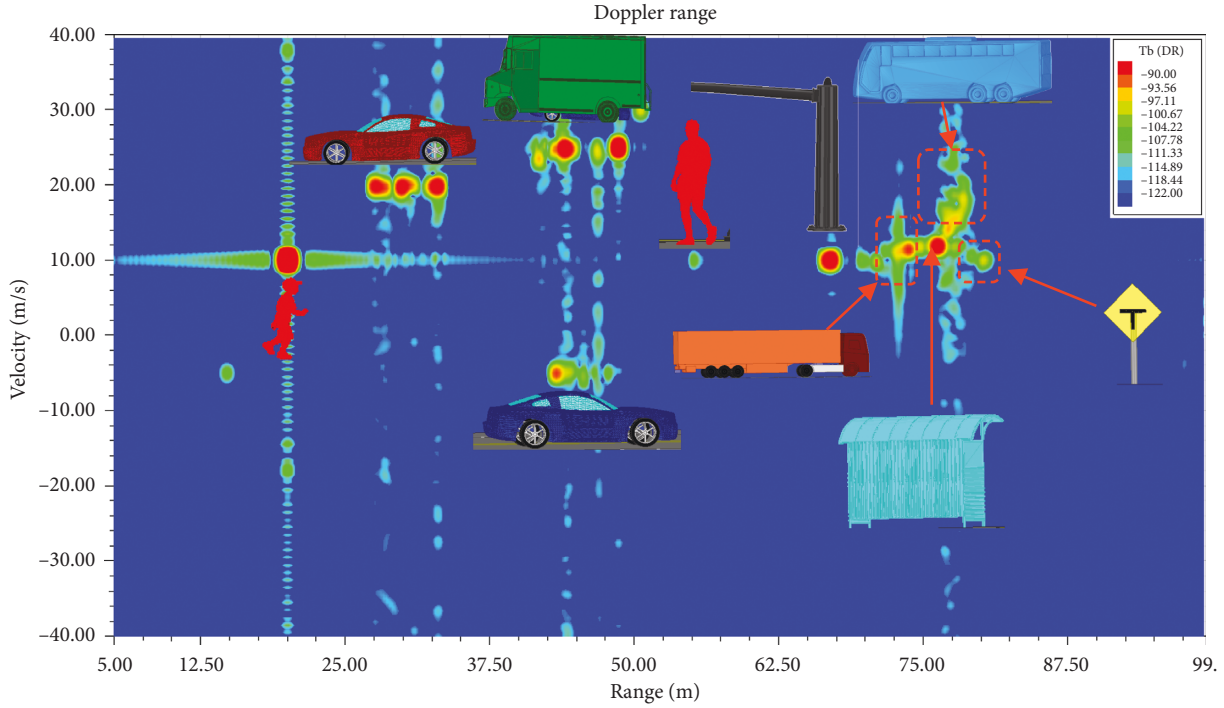

Figure 11: Range-Doppler map for the radar scene shown in Figure 10. Here, each target appears as a strong return at the correct range/velocity point. Although the pedestrian boy is a small target, he shows strong returns since he is 20 meters away.

plots. Of interest is how this full physics-based result has been obtained without fabricating a single component. To demonstrate the ray-tracing aspect of this simulation, a visual ray-trace plot was obtained for the scene in Figure 10. The visual ray-trace plot (VRT) shows all the paths taken by the geometric optic rays as they travel from the transmitter to the targets along with the subsequent bounces of these targets. Figure 12 shows a VRT plot for the scene shown in Figure 10.

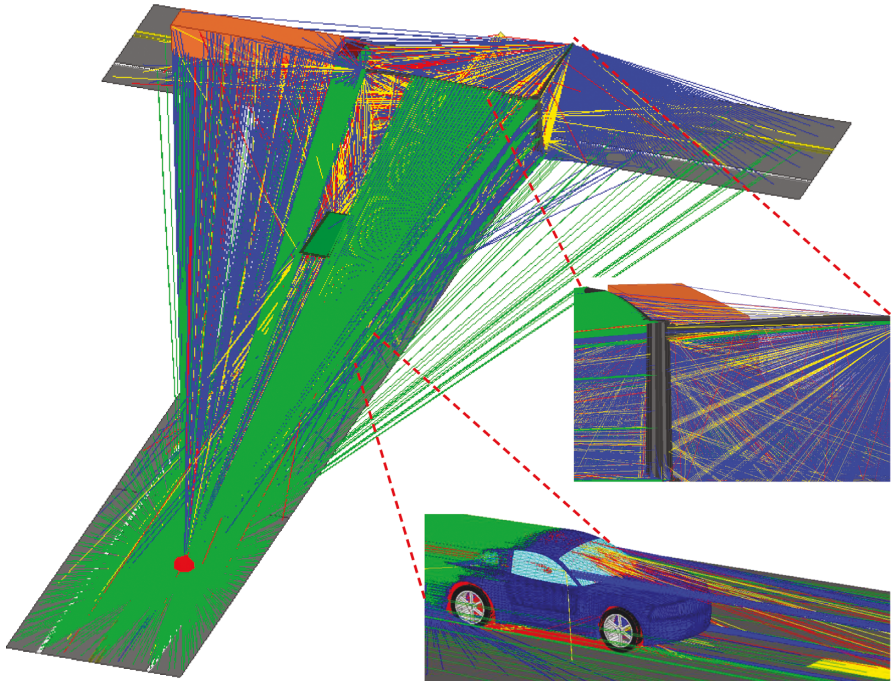

Figure 12: Visual ray-tracing plot for radar scene shown in Figure 10. Note: the different colors correspond to different bounces that the ray has encountered. Green (1 bounce), blue (2 bounces), yellow (3 bounces), and red (4 bounces).

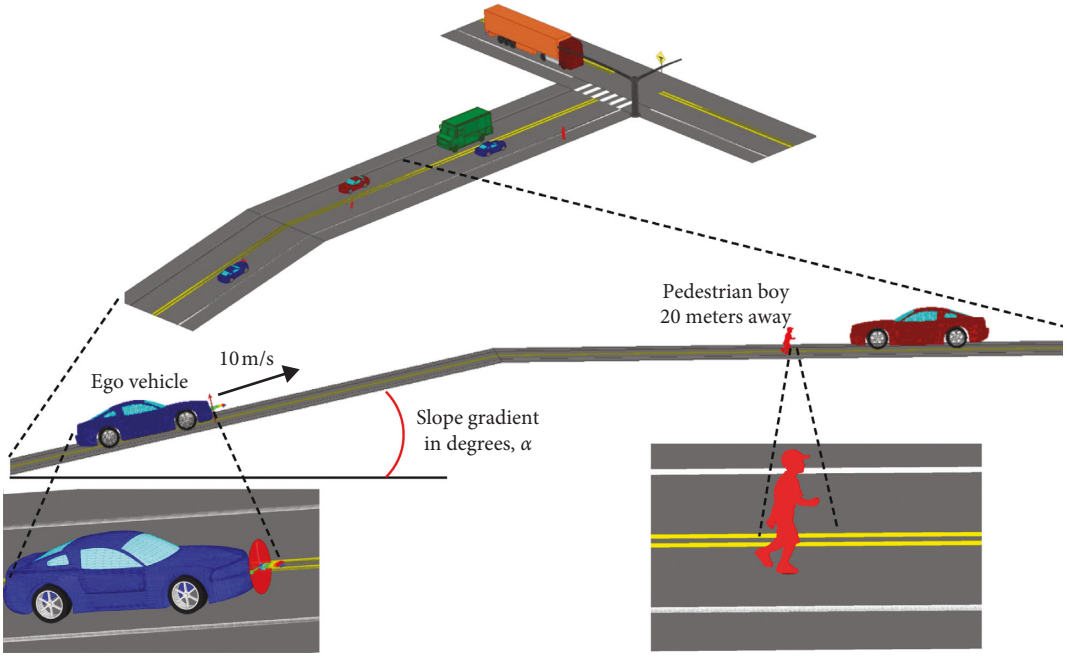

Figure 13: Simulation setup for investigating the effects of slopes on radar returns. The target of interest is the pedestrian boy directly ahead of the oncoming ego vehicle. The slope gradient α will be varied in the study while radar returns are recorded.

5. Investigating Automotive Corner Cases

In almost every aspect of engineering, there exist some corner cases that may or may not have significant consequences. Corner cases represent specific situations that exist outside of normal operation parameters. In automotive radar, the investigation of corner cases is of extreme importance as it can provide engineers with valuable insight into how corner case effects can be mitigated. In the case where automotive radar fails, corner case investigation can possibly tell engineers and investigators alike what may have occurred. Typical examples of corner cases for automotive radar are the effects of guard rails, tunnels, and sensor heating on radar returns. As the vehicle evolves from merely

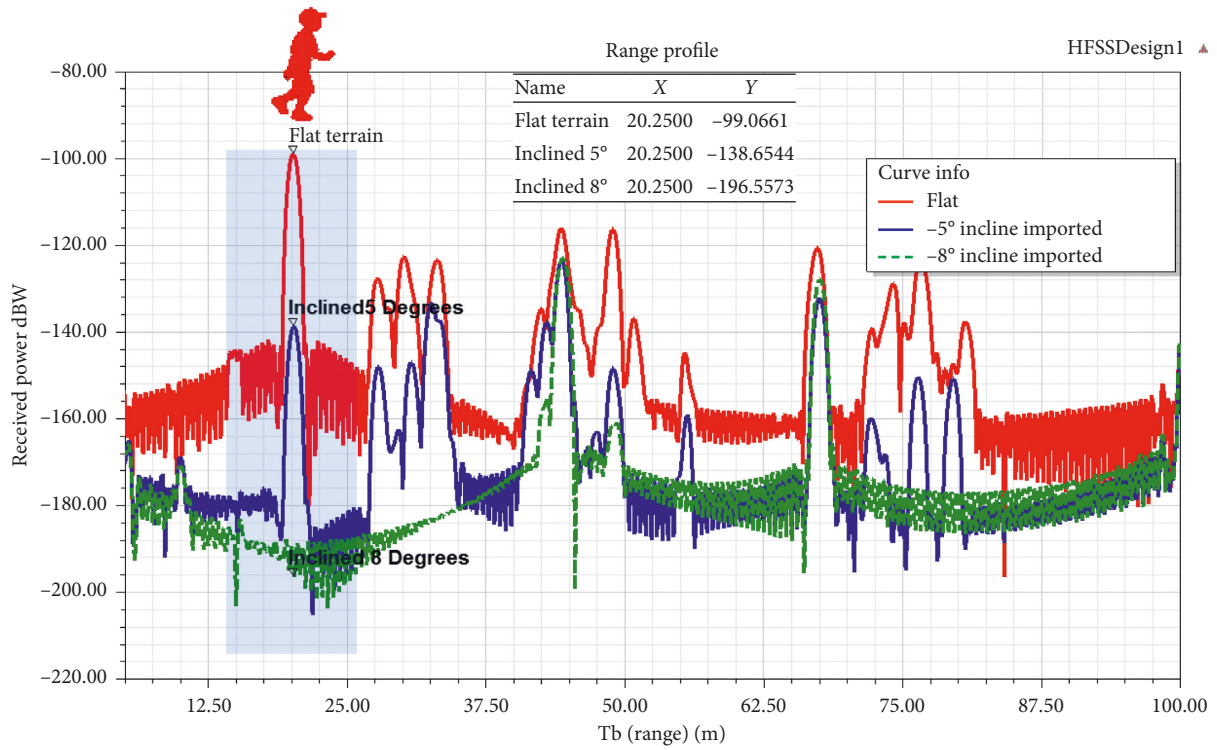

Figure 14: Radar range profiles for different road incline angles (see Figure 13). The pedestrian boy radar returns have been highlighted, and they completely disappear at $\alpha = 8^{\circ}$.

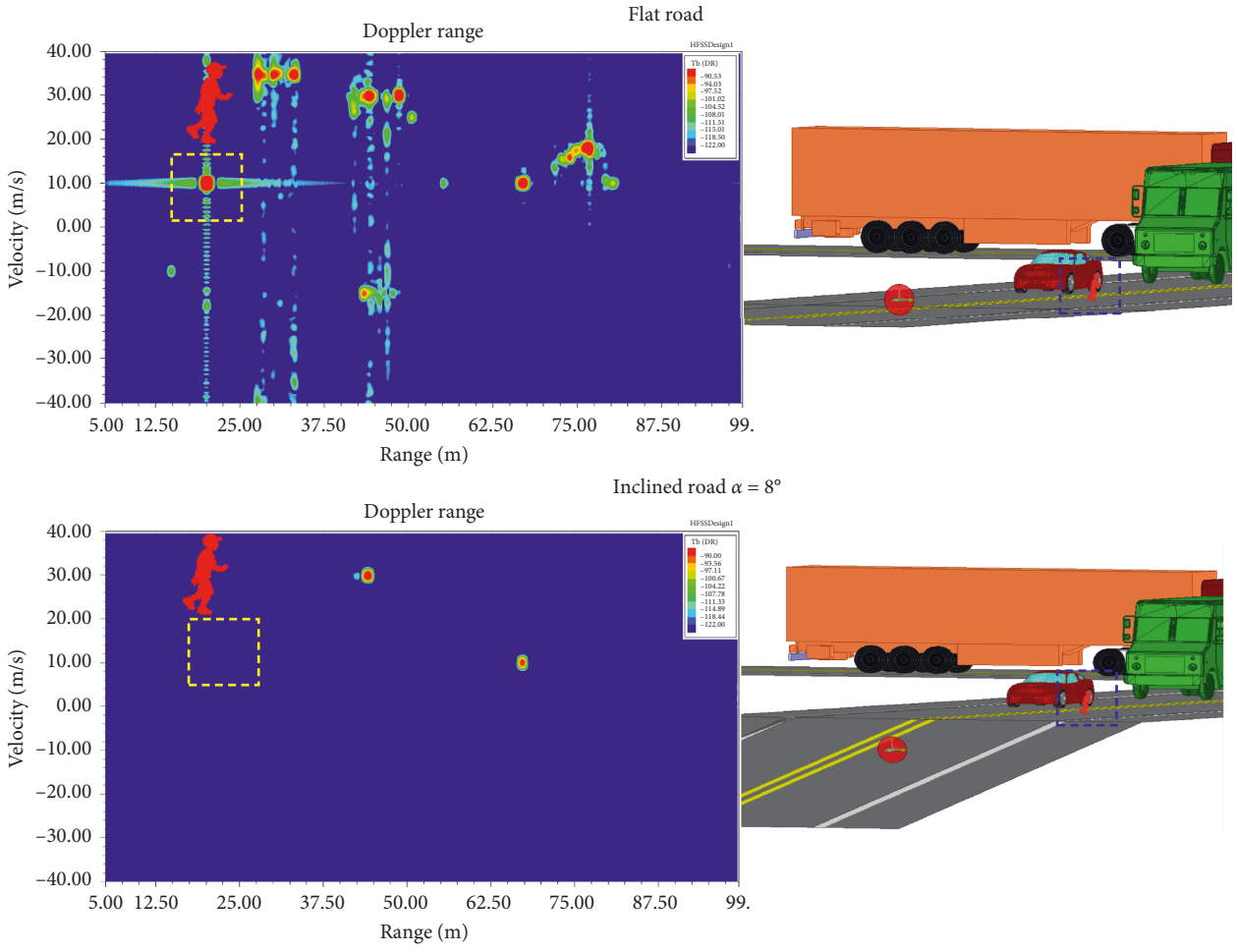

Figure 15: Range-Doppler maps for flat and inclined ground returns. Notice how multiple targets including a pedestrian boy directly ahead of the ego vehicle disappear. Note: the same scale was used for both the figures.

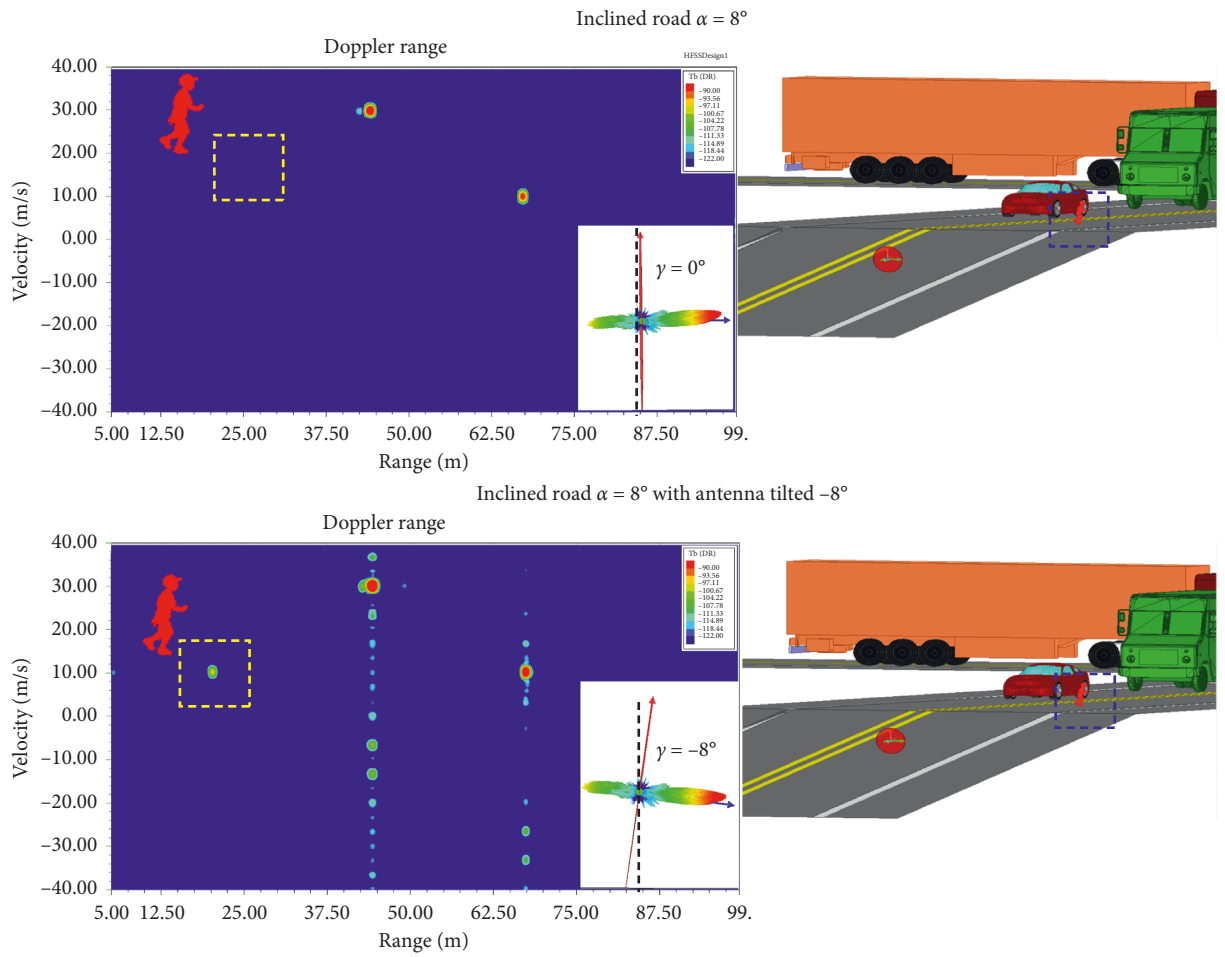

FIGURE 16: Mitigating slope-induced reduced radar returns using a slope compensating angle γ. Notice how the previously invisible pedestrian target reappears when the antennas are slightly tilted. Note: the same scale was used for both the figures.

assisting the driver to becoming fully autonomous, the corner case response of all ADAS components will need to be extremely reliable. Simulation is the only practical way to investigate the myriad of potential corner cases.

System-level simulators can provide valuable insight into how the overall system will behave if some parameters change. This is perfect for systems operating under normal conditions; however, non-full physics-based solvers fall short when investigating automotive radar corner cases. At its core, the radar problem is inherently an electromagnetic propagation problem. Therefore, full physics electromagnetic solvers are needed to investigate automotive radar corner cases. In this section, two corner cases and possible mitigation techniques will be presented. The first case investigates terrain slope-induced reduced radar returns and its impact on early target detection. The second case investigates false target detection due to metallic road construction plates. Each of these corner cases represents a situation where full physics simulation of radar scenes can provide potentially lifesaving insight.

5.1. Case 1: Terrain Slope-Induced Reduced Radar Returns. Driving on high gradient or undulating roads can be challenging for a driver. This is because forward visibility is extremely limited by the rapidly varying terrain. Automotive radar is also adversely affected by undulating roads or high gradient slopes. Cities such as San Francisco are notorious for having steep streets such as Filbert Street and 22nd Street that have gradients of up to 17.5°. The radar sensor is mounted on the vehicle, which, depending on the nature of the slope, may be facing up or down relative to flat terrain. In these cases, the radar sensor itself is also "facing" either up or down. It will be shown how certain targets can disappear from the radar range-Doppler map. This can have devastating effects due to the radar "overlooking" critical targets such as pedestrians and vehicles ahead. In bad weather conditions, the autonomous vehicle will predominantly depend on radar for target identification; therefore, target visibility on high gradient roads is of extreme importance.

A crucial corner case occurs when a vehicle is approaching a flat terrain from a positive gradient slope. Here, the vehicle and radar sensor are essentially facing upwards as shown in Figure 13.

Using the model in Figure 13, the radar returns for different slope angles were investigated. The slope was varied until the pedestrian child disappeared from the radar range plot. Figure 14 shows the radar range plots for different

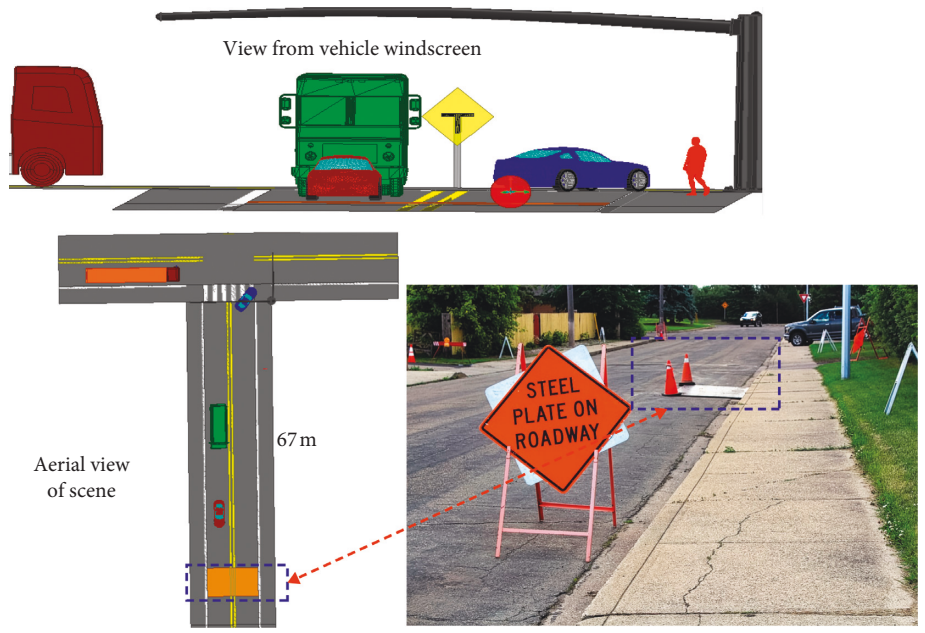

FIGURE 17: Simulation setup for investigating the effects of steel plate road coverings. Notice how the nearest vehicle in the ego vehicle's lane is 67 m away. With an empty lane ahead, optical cameras would see the lane as an empty one.

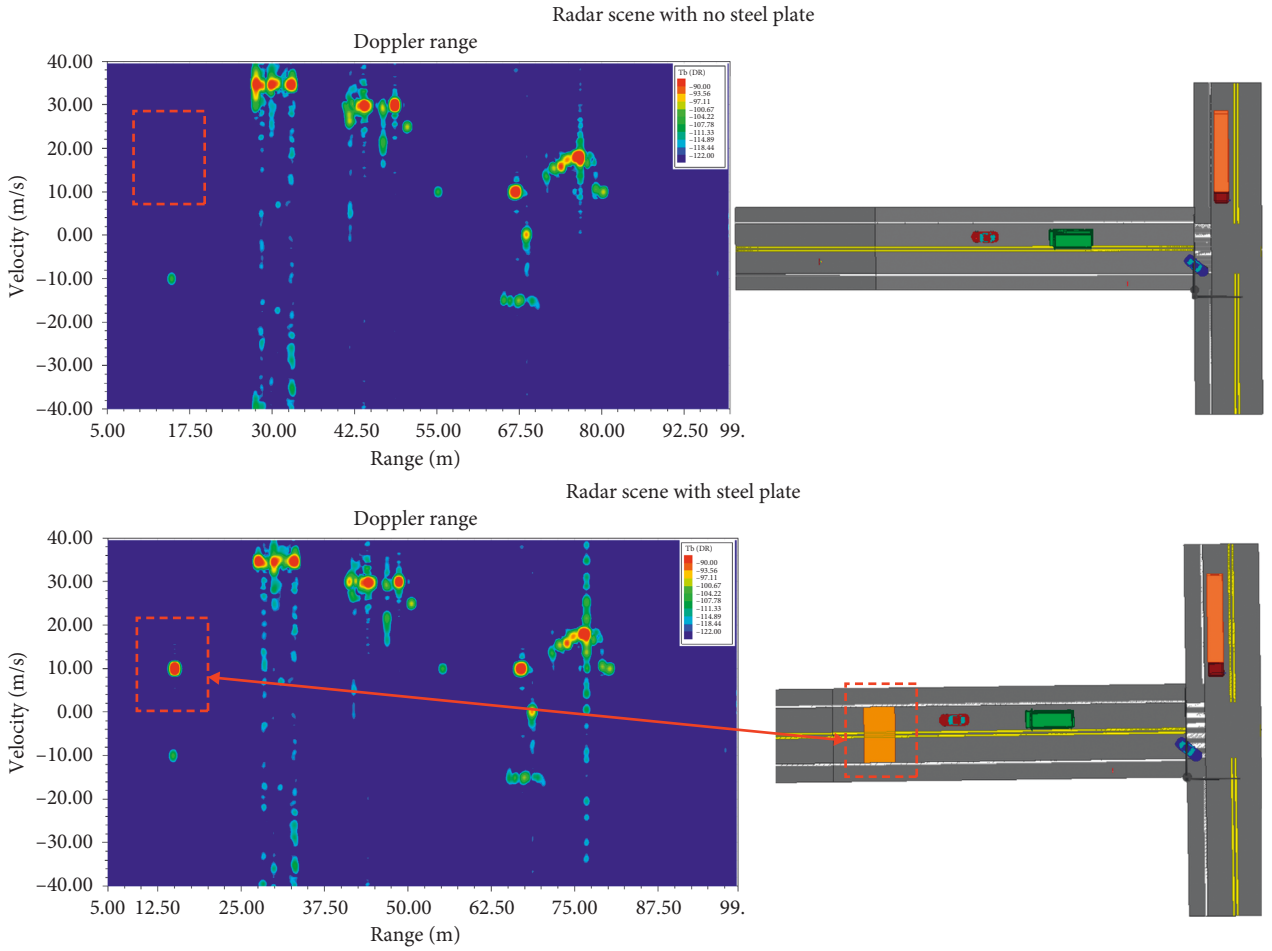

FIGURE 18: Range-Doppler maps for two scenes with and without a construction steel plate. Due to diffraction effects, current discontinuities at the plate edges reradiate and are presented as strong returns to the radar. Note: the same scale was used for both the figures.

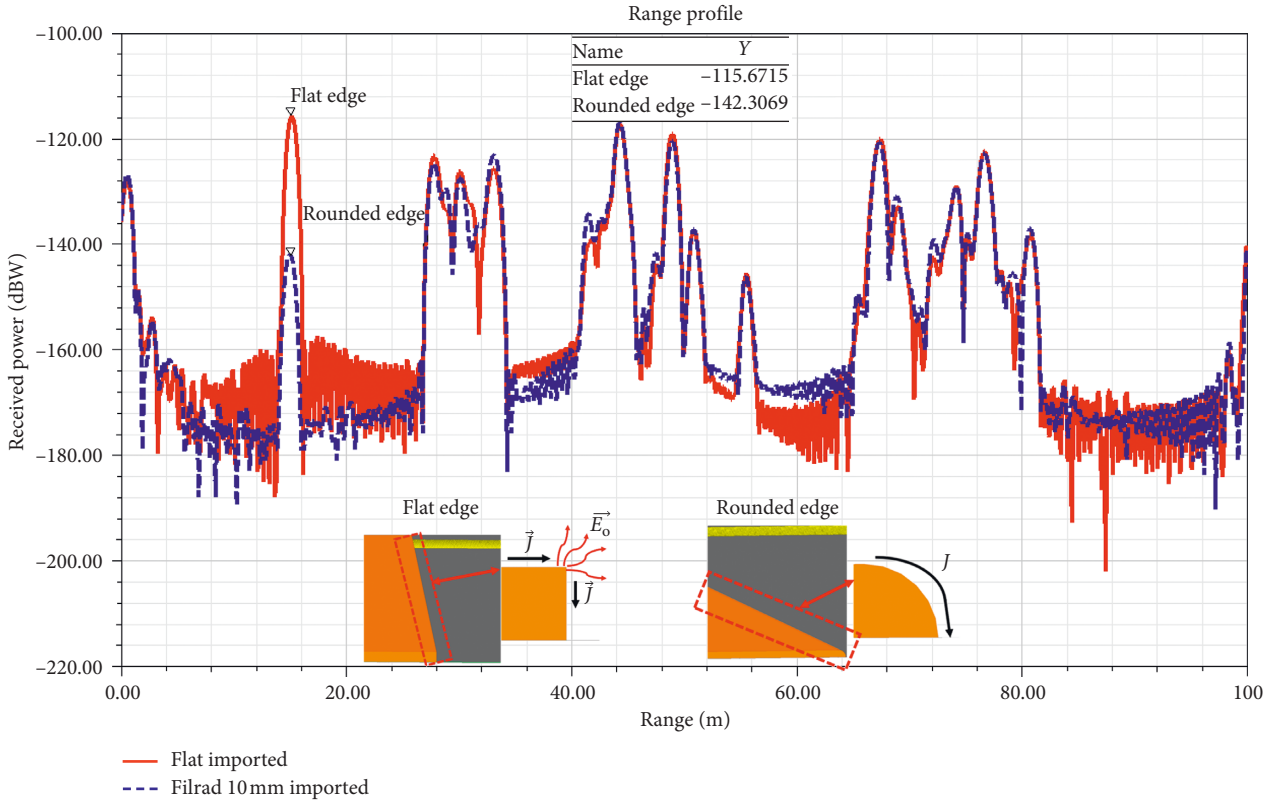

FIGURE 19: Range profiles for radar scene shown in Figure 17. Steel plates with flat edges have a larger RCS due to diffraction. Rounding the edges as shown above significantly reduces the steel plate RCS by mitigating diffraction effects.

slopes. Here, $\alpha = 0$ refers to flat ground. As can be seen from Figure 14, at a slope of approximately $\alpha = 8^{\circ}$, the radar returns of the pedestrian boy vanish with an almost 100 dB drop. Results from this simulation predict the possibility of a catastrophic situation in which automotive radar may fail to detect crucial targets that are slightly beyond the horizon.

To further demonstrate the extreme reduction of radar returns due to the slope, range-Doppler maps for flat terrain and $\alpha = 8^{\circ}$ were simulated and are shown in Figure 15. Of interest is how multiple targets disappear when the ego vehicle is tilted relative to the terrain it is approaching. Note that the same plot scale was maintained for all the range-Doppler maps in this paper.

Results from Figures 14 and 15 demonstrate the need for techniques that mitigate the radar return reduction. For a vehicle travelling at 22 mph (10 m/s), it typically takes 14 meters from the moment brakes are applied to come to a complete stop. Therefore, early detection of a target beyond the slope horizon may prevent accidents or pedestrian fatalities. A proposed early detection technique is to tilt the radar sensor in the elevation plane to compensate for the upward gradient. The idea is for the antennas to "look" down when the vehicle is looking up. By using multiple TX antennas that are staggered in the elevation, beam scanning can be achieved using phase shifting. The beam scanning system would be connected to a gyroscope or slope detection sensor. To test the effectiveness of this system, a compensation angle γ of rotation along the elevation plane was added to both the TX and RX antennas. This angle was varied until peak radar returns were obtained. Figure 16 shows the range-Doppler map for a radar system with a slope compensation tilting system. As seen from Figure 16, by tilting the radar system, the previously invisible pedestrian can now be detected. Results from simulation demonstrate that a compensation angle equal to the negative slope angle is optimum, that is, $\gamma = -\alpha$. Such an early target detection technique has the potential to save pedestrians and prevent accidents.

5.2. Case 2: False Target Detection Caused by Construction Metal Plates. Target detection and tracking is the fundamental goal of any radar system. Early target detection can help ADAS to provide the driver with warnings such as vehicles in the blind spot. In fully autonomous vehicle operation, early target detection can allow the vehicle to engage collision avoidance protocols. While failure to detect a target can be catastrophic, detecting a false target can be equally disastrous for autonomous vehicles. Specifically, any false target detected by the radar system can force the car into collision avoidance maneuvers that could cause an accident. Adaptive cruise control (ACC) systems are particularly susceptive to the effects of false targets. These systems are designed to maintain a specific speed while monitoring the road ahead; if the vehicle ahead slows down, the ego vehicle will slow down as well. Accidents arise when the ACC system identifies false targets that force it to engage the automatic emergency brake (AEB) system. Sudden engagement of the AEB system due to targets

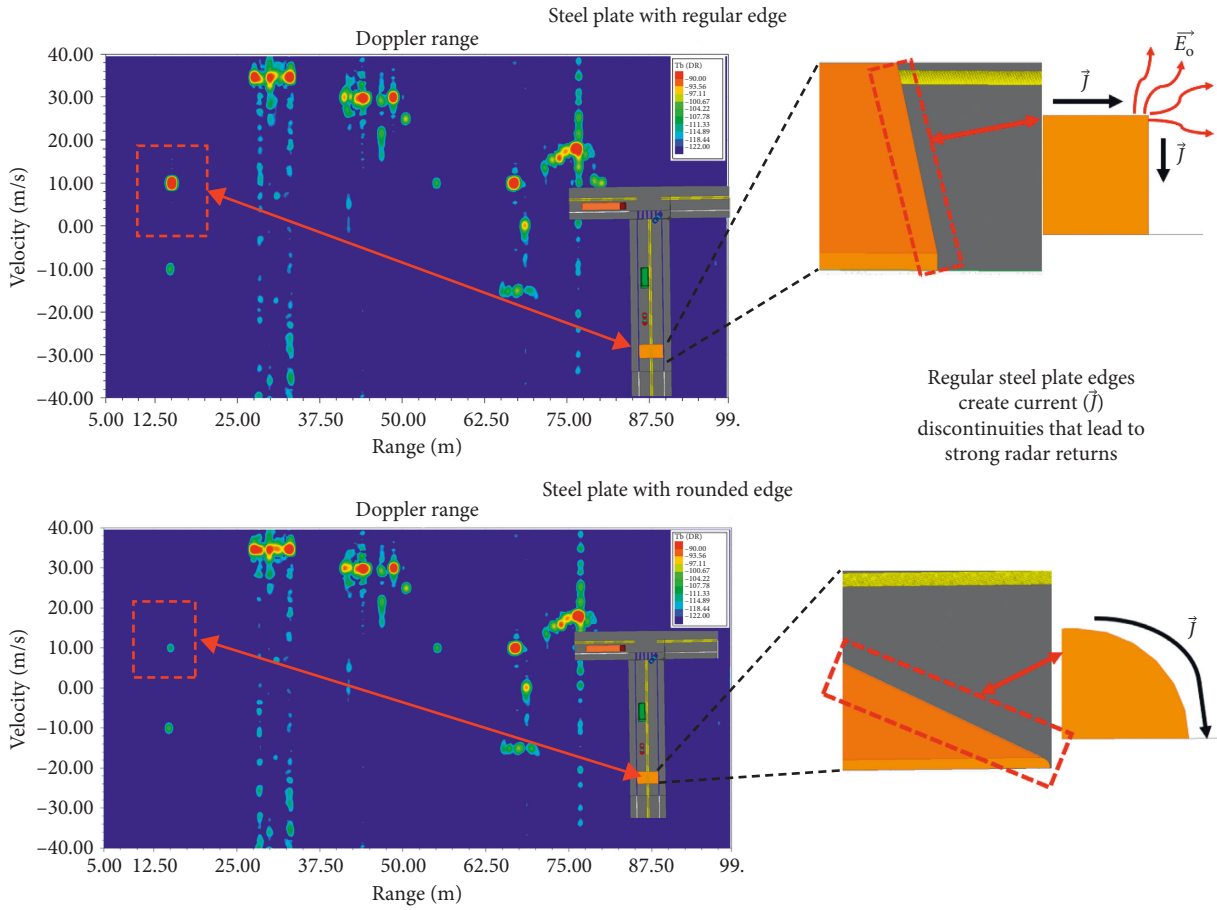

Figure 20: Range-Doppler plots for different edge finishes of construction steel plates. Rounded edges significantly reduce the RCS of the metal plate by reducing diffraction effects. Smooth edges have less current ($\vec{j}$) discontinuities. Note: the same scale was used for both the figures.

that other drivers do not perceive to be present can lead to rear-end collisions. Because the radar problem is inherently an electromagnetic wave transmission and reflection problem, regular objects encountered on the roads can present extremely strong returns. Examples of these objects are street signs and guard rails. In this corner case study, the radar returns of construction metallic plates are investigated.

When laying down cables or utility pipes, construction companies often dig trenches in streets. These trenches are typically covered with metallic plates to allow vehicles to still use those streets during construction. Although these plates are only 25 mm thick, at 77 GHz, their edges present the radar with a 6λ (6 electrical wavelengths) thick target. To investigate the impact of the steel plates, a radar scene was created in HFSS. Figure 17 shows the construction steel plates and an HFSS SBR+ radar scene. Included in the scene is a 9 × 5-m steel plate with a 10-mm thickness (~2.5λ). This plate was placed directly in the lane of the ego vehicle. The rest of the lane was intentionally left empty, except for the turning blue vehicle 67 meters away.

Figure 18 shows the range-Doppler maps for the scene shown in Figure 17 with and without the steel plate. It is interesting to note how the steel plate presents a very strong target for the radar sensor. This target strength is comparable to that of actual vehicles.

Edge reflection and corner diffraction at the metal edges are the culprits. The metal edge face presents a fairly large surface area at 77 GHz. On the other hand, steel plate edges present a sharp edge where a current discontinuity occurs. It is this current discontinuity that then reradiates. This reradiation presents itself as a strong target return for the radar. To prevent automotive radars from picking up this false target, the RCS of the steel plate needs to be reduced. One solution can be to cover the metallic plates with W band (75 GHz–110 GHz) absorbers [39]; however, it would be both impractical and expensive to coat construction steel plates with these absorbers.

We propose a method of reducing the steel plate RCS by mitigating diffraction at the plate edges and reducing the flat face of the facing surface. Curving the edges is an effective way of reducing diffraction because it leads to the elimination of current discontinuities. Figure 19 shows the radar range plot of the scene shown in Figure 17. Here, two types of steel plates are used. The first steel plate is the regular plate with square edges. The second plate has the same thickness, length, and width. However, its edges are rounded to mitigate diffraction effects. As seen in Figure 19, rounding the

edges of the steel plates can reduce the radar return intensity by 27 dB (~500x reduction). Figure 20 shows the range-Doppler map for the regular plate and for the rounded plate. The rounded edges significantly reduce the returns of construction plates. Such a weak target can be filtered out by the vehicle's target detection algorithm with ease. By being able to filter out the rounded steel plates, potential accidental automatic emergency braking can be avoided. This is a significant result that shows the need for cooperation between automotive makers and infrastructure construction companies. Such corner cases can only be tested in the field or simulated using full physics-based solvers.

6. Conclusion

77 GHz automotive radar is one of the key sensors required to develop reliable active safety systems for fully autonomous vehicles. To demonstrate reliability, simulation has emerged as the only practical solution to reduce or eliminate cost and time constraints associated with building and testing physical prototypes. In this paper, HFSS FEM was used for antenna design, optimization, and radome effects analysis. HFSS SBR+ was then used to investigate the effects of the bumper and car-facia interaction on the antenna radiation characteristics. A full-scale radar scene was then modelled in HFSS SBR+ and analyzed. Range plots and range-Doppler plots were presented for a complex traffic scene. Two automotive radar corner cases were investigated. A technique for mitigating road-slope-induced reduced radar returns was proposed and validated. Using full physics simulations, it was demonstrated how this technique can lead to early detection of pedestrians and potentially save lives. Finally, a technique for reducing the RCS of road construction metal plates was proposed to avoid accidental automatic emergency braking due to false target detection. This work shows how an entire automotive radar workflow can be simulated to develop optimal sensors, to account for installation effects, and to investigate active safety systems corner cases.

Data Availability

The ANSYS Electronic Desktop (AEDT) files that were used to support the findings of this study are available from the corresponding author (ushe.chipengo@ansys.com) upon request. Interested individuals must have HFSS SBR+ to be able to open the files. The authors retain the right to not disclose any information that may be deemed proprietary.

Conflicts of Interest

The authors declare that there are no conflicts of interest regarding the publication of this paper.

References

[1] A. K. Yadav and J. Szpytko, "Safety Problems in vehicles with adaptive cruise control system," *Journal of KONBiN*, vol. 42, no. 1, pp. 389–398, 2017.

[2] R. Sagar, "Making cars safer through technology innovation," *Texas Instruments*, pp. 1–10, 2017.

[3] J. Hasch, E. Topak, R. Schnabel, T. Zwick, R. Weigel, and C. Waldschmidt, "Millimeter-wave technology for automotive radar sensors in the 77 GHz frequency band," *IEEE Transactions on Microwave Theory and Techniques*, vol. 60, no. 3, pp. 845–859, 2012.

[4] D. M. Gavrila, "The visual analysis of human movement: a survey," *Computer Visual Image Understanding*, vol. 73, no. 1, pp. 82–98, 1999.

[5] T. B. Moeslund and E. Granum, "A survey of advances in vision-based human motion capture and analysis," *Computer Visual Image Understanding*, vol. 104, no. 2-3, pp. 90–126, 2006.

[6] R. Poppe, "Vision based human motion analysis: an overview," *Computer Visual Image Understanding*, vol. 108, no. 1-2, pp. 4–18, 2007.

[7] R. H. Rasshofer and K. Gresser, "Automotive radar and lidar systems for next generation driver assistance functions," *Advances in Radio Science*, vol. 3, pp. 205–209, 2005.

[8] G. Reina, D. Johnson, and J. Underwood, "Radar sensing for intelligent vehicles in urban environments," *Sensors*, vol. 15, no. 6, pp. 14661–14678, 2015.

[9] S. Patole, M. Torlak, D. Wang, and M. Ali, "Automotive radars: a review of signal processing techniques," *IEEE Signal Processing Magazine*, vol. 34, no. 2, pp. 22–35, 2017.

[10] K. Ohguchi, M. Shono, and M. Kishida, "79 GHz band ultra-wideband automotive radar," *Fujitsu Ten Technical Journal*, vol. 39, pp. 9–14, 2013.

[11] J. Singh, B. Ginsburg, S. Rao, and K. Ramasubramanian, "AWR1642 mmWave sensor: 76–81 GHz radar-on-chip for short range radar applications," *Texas Instruments*, pp. 1–7, 2017.

[12] K. Ramasubramanian, K. Ramaiah, and A. Aginskiy, "Moving from legacy 24 GHz to state-of-the-art 77 GHz radar," *Texas Instruments*, pp. 1–6, 2017.

[13] B. H. Ku, P. Schmalenberg, O. Inac et al., "A 77-81 GHz 16 element phased-array receiver with ±50° beam scanning for advanced automotive radars," *IEEE Transactions on Microwave Theory and Techniques*, vol. 62, no. 11, pp. 2823–2831, 2014.

[14] Altera Corporation, *Implementing digital processing for automotive radar using SoCs*, Altera Corporation, San Jose, CA, USA, 2013.

[15] R. Gourova, O. Krasnov, and A. Yarovoy, "Analysis of rain clutter detections in commercial 77 GHz automotive radar," in *Proceedings of the 14th European Radar Conference*, pp. 25–28, Nuremberg, Germany, October 2017.

[16] H. Kim, H. Lee, J. Cho, and C. Kim, "Beam expansion of blind spot detection radar antennas using a radome with defected corrugated inner wall," *International Journal of Antennas and Propagation*, vol. 2017, Article ID 7316282, 12 pages, 2017.

[17] T. Kim and B. Song, "Detection and tracking of road barrier based on radar and vision sensor fusion," *Journal of Sensors*, vol. 2016, Article ID 1963450, 8 pages, 2016.

[18] T. Chen, H. Wu, and L. Liu, "A joint Doppler frequency shift DOA estimation algorithm based on sparse representations for collocated TDM-MIMO radar," *Journal of Applied Mathematics*, vol. 2014, Article ID 421391, 9 pages, 2014.

[19] Y.-D. Kim, G.-J. Son, C.-H. Song, and H.-K. Kim, "On the deployment and noise filtering of vehicular radar application for detection enhancement in roads and tunnels," *Sensors*, vol. 18, no. 3, pp. 1–21, 2018.

[20] G. A. Casula, G. Mazzarella, and G. Montisci, "A truncated waveguide fed by a microstrip as a radiating element for high

performance automotive anti-collision radars radars," *International Journal of Antennas and Propagation*, vol. 2012, Article ID 983281, 9 pages, 2012.

[21] C. Balanis, *Advanced Engineering Electromagnetics*, John Wiley & Sons, Inc., Hoboken, NJ, USA, 2012.

[22] J. H. Lee, J. M. Lee, and K. C. Hwang, "Series feeding rectangular microstrip patch array antenna for 77 GHz automotive radar," in *Proceedings of the 2017 International Symposium on Antennas and Propagation (ISAP2017)*, pp. 1-2, Phuket, Thailand, October-November 2017.

[23] W. Menzel and A. Moebius, "Antenna concepts for millimetre-wave automotive radar sensors," *Proceedings of the IEEE*, vol. 100, no. 7, pp. 2372–2379, 2012.

[24] J. Xu, W. Hong, H. Zhang et al., "An Array antenna for both long and medium range 77 GHz automotive radar applications," *IEEE Transactions on Antennas and Propagation*, vol. 65, no. 12, pp. 7207–7216, 2017.

[25] J. Freese, R. Jakoby, H. L. Blocher, and J. Wenger, "Synthesis of microstrip series fed-patch arrays for 77 GHz-sensor applications," in *Proceedings of 2000 Asia-Pacific Microwave Conference*, Sydney, Australia, December 2000.

[26] T. Yuan, N. Yuan, and L. W. Li, "A novel, series-fed taper antenna array design," *IEEE Antennas and Wireless Propagation Letters*, vol. 7, pp. 362–365, 2008.

[27] J. Schoebel and P. Herrero, "Planar antenna technology for mm-Wave automotive radar, sensing and communications," in *Radar Technology, Chapter 15*, Intech, London, UK, 2009.

[28] S. H. Jeong, H. Y. Yu, J. E. Lee, J. N. Oh, and K. H. Lee, "A multibeam and multi-range radar with FMCW and digital beam forming for automotive applications," *Progress in Electromagnetics Research*, vol. 124, pp. 285–299, 2012.

[29] Y. I. Chong and D. Wenbin, "Microstrip series fed antenna array for millimetre wave automotive radar applications," in *Proceedings of 2012 IEEE MTT-S International Microwave Workshop Series on Millimeter Wave Wireless Technology and Applications*, pp. 18–20, Nanjing, China, September 2012.

[30] S. Khan and D. C. Dubkariya, "Design of series feed microstrip antenna array for low side lobe level," *International Journal of Electronics and Communication Technology*, vol. 6, no. 3, pp. 45–47, 2015.

[31] C. Callewaert, "On the radar," *ANSYS Advantage Magazine*, vol. 12, no. 1, pp. 24–27, 2018.

[32] S. Carpenter, "Autonomous vehicle radar," *ANSYS Advantage Magazine*, vol. 12, no. 1, pp. 32–37, 2018.

[33] ANSYS Savant 2018.2, *Help Section: Theory*, ANSYS, Canonsburg, PA, USA, 2018.

[34] R. M. Scheer and J. Holm, *Principles of Modern Radar Edison*, SCITech Publishing, Mendham, NJ, USA, 2010.

[35] C. Iovescu and S. Rao, *The fundamentals of millimetre wave sensors*, Texas Instruments, Dallas, TX, USA, 2017.

[36] A. Sligar, *ANSYS HFSS R19: Radar Processing, the RadarPre and RadarPost ACT Extension*, ANSYS, Canonsburg, PA, USA, 2018.

[37] T. Wu, T. S. Rappaport, and C. M. Collins, "The human body and millimetre-wave wireless communication systems: interactions and implications," in *Proceedings of 2015 IEEE International Conference on Communications (ICC)*, pp. 1–7, London, UK, June 2015.

[38] D. Belgiovane, C. Chen, M. Chen, S. Y. P Chien, and R. Sherony, "77 GHz Radar scattering properties of pedestrians," in *Proceedings of 2014 IEEE Radar Conference*, Cincinnati, OH, USA, May 2014.

[39] D. Green and J. Marchand, *Focusing in on W-Band absorbers*, ARC Technologies, Amesbury, MA, USA, 2015.